Noncatalytic chalcone isomerase-fold proteins in *Humulus lupulus* are auxiliary components in prenylated flavonoid biosynthesis

Zhaonan Ban[a,b], Hao Qin[a], Andrew J. Mitchell[c], Baoxiu Liu[a], Fengxia Zhang[a], Jing-Ke Weng[c,d], Richard A. Dixon[e,f,1], and Guodong Wang[a,1]

[a]State Key Laboratory of Plant Genomics and National Center for Plant Gene Research, Institute of Genetics and Developmental Biology, Chinese Academy of Sciences, 100101 Beijing, China; [b]University of Chinese Academy of Sciences, 100049 Beijing, China; [c]Whitehead Institute for Biomedical Research, Cambridge, MA 02142; [d]Department of Biology, Massachusetts Institute of Technology, Cambridge, MA 02139; [e]BioDiscovery Institute, University of North Texas, Denton, TX 76203; and [f]Department of Biological Sciences, University of North Texas, Denton, TX 76203

Contributed by Richard A. Dixon, April 25, 2018 (sent for review February 6, 2018; reviewed by Joerg Bohlmann and Mattheos A. G. Koffas)

Xanthohumol (XN) and demethylxanthohumol (DMX) are specialized prenylated chalconoids with multiple pharmaceutical applications that accumulate to high levels in the glandular trichomes of hops (*Humulus lupulus* L.). Although all structural enzymes in the XN pathway have been functionally identified, biochemical mechanisms underlying highly efficient production of XN have not been fully resolved. In this study, we characterized two noncatalytic chalcone isomerase (CHI)-like proteins (designated as HlCHIL1 and HlCHIL2) using engineered yeast harboring all genes required for DMX production. HlCHIL2 increased DMX production by 2.3-fold, whereas HlCHIL1 significantly decreased DMX production by 30%. We show that CHIL2 is part of an active DMX biosynthetic metabolon in hop glandular trichomes that encompasses a chalcone synthase (CHS) and a membrane-bound prenyltransferase, and that type IV CHI-fold proteins of representative land plants contain conserved function to bind with CHS and enhance its activity. Binding assays and structural docking uncover a function of HlCHIL1 to bind DMX and naringenin chalcone to stabilize the ring-open configuration of these chalconoids. This study reveals the role of two HlCHILs in DMX biosynthesis in hops, and provides insight into their evolutionary development from the ancestral fatty acid-binding CHI-fold proteins to specialized auxiliary proteins supporting flavonoid biosynthesis in plants.

chalcone isomerase-like | chalcone synthase | flavonoid | *Humulus lupulus* | trichome

Hops (*Humulus lupulus* L., Cannabaceae) is a dioecious perennial vine, whose female cones are a key ingredient that provide unique flavor and aroma for brewing beer. Essential oils, bitter acids, and prenylchalcones account for the major three categories of specialized metabolites that are highly accumulated in the glandular trichomes (lupulin glands) of female cones, while different combinations of these compounds dictate the bittering and finishing of beer (1–3). Trace amounts of prenylated flavanones have also been detected in hops (4). Recent studies have demonstrated that hop terpenophenolics (a term for both bitter acids and prenylchalcones) exhibit diverse bioactivities with a high potential for pharmaceutical applications (5–8) (Fig. 1), with the prenylchalcones exhibiting higher bioactivity than the prenylflavanones, mainly due to the α,β- unsaturated ketone functional group in chalcones (9–11). Among these prenylchalcones, xanthohumol (XN, 3′-prenyl-6′-*O*- methylchalconaringenin) (Fig. 1) has received much attention due to its cancer-preventive, antiinflammatory, and antioxidant properties (3, 12–16). XN exhibits more powerful antioxidant activity than resveratrol, the well-known antioxidant found naturally in red wine (17).

To understand the molecular basis for the biosynthesis of terpenophenolics in hop trichomes, a total of more than 22,000 expressed sequence tags (ESTs) from several hop trichome-specific cDNA libraries have been deposited in the TrichOME database [www.planttrichome.org (18)], and numerous large RNAseq datasets from different hop tissues or cultivars have also been made publically available. By mining the hops transcriptome data, we and others have functionally identified several key terpenophenolic biosynthetic enzymes from hop glandular trichomes (1, 18–23); these include carboxyl CoA ligase (CCL) genes and two aromatic prenyltransferase (PT) genes (*HlPT1L* and *HlPT2*) (22, 23). We have shown that HlPT2 physically interacts with HlPT1L to form an active metabolon that catalyzes the major prenylations in the β-bitter acid pathway with high efficiency: PT1L catalyzes the first prenylation step and PT2 catalyzes the subsequent two prenylation steps. We then successfully reconstructed the whole β-bitter acid pathway by coexpressing two CoA ligases (*HlCCL2* and *HlCCL4*), the polyketide synthase valerophenone synthase (*HlVPS*), and the dimethylallyl diphosphate (DMAPP)-consuming PT complex in an optimized yeast system (*DD104* strain, in which the endogenous farnesyl pyrophosphate synthase activity was down-regulated by site-mutation of K197G) (23).

In XN biosynthesis, *p*-coumaroyl-CoA is produced by the sequential actions of L-Phe ammonia-lyase (PAL), cinnamate 4-hydroxylase (C4H), and *p*-coumaroyl-CoA ligase (HlCCL1 from hops) (Fig. 1). Chalcone synthase (CHS; EC 2.3.1.74) then catalyzes the condensation of *p*-coumaroyl-CoA with malonyl-CoA to form naringenin chalcone (NC). A trichome-specific *CHS*

Significance

Here, we identify two noncatalytic chalcone isomerase-fold proteins, which are critical for high-efficiency prenylchalcone production in *Humulus lupulus*. Our results provide insights into their evolutionary development from the ancestral noncatalytic fatty acid-binding chalcone isomerase-fold proteins to specialized auxiliary proteins supporting flavonoid biosynthesis in plants, and open up the possibility of producing high-value plant prenylchalcones using heterologous systems.

Author contributions: R.A.D. and G.W. designed research; Z.B., A.J.M., and B.L. performed research; H.Q. and F.Z. contributed new reagents/analytic tools; Z.B., J.-K.W., and G.W. analyzed data; and Z.B. and G.W. wrote the paper.

Reviewers: J.B., University of British Columbia; and M.A.G.K., Rensselaer Polytechnic Institute.

The authors declare no conflict of interest.

Data deposition: The sequences reported in this paper have been deposited in the GenBank database (accession nos. HlCHIL1, HlCHIL2, MG324004, and MG324005).

[1]To whom correspondence may be addressed. Email: Richard.Dixon@unt.edu or gdwang@genetics.ac.cn.

This article contains supporting information online at www.pnas.org/lookup/suppl/doi:10.1073/pnas.1802223115/-/DCSupplemental.

Published online May 14, 2018.

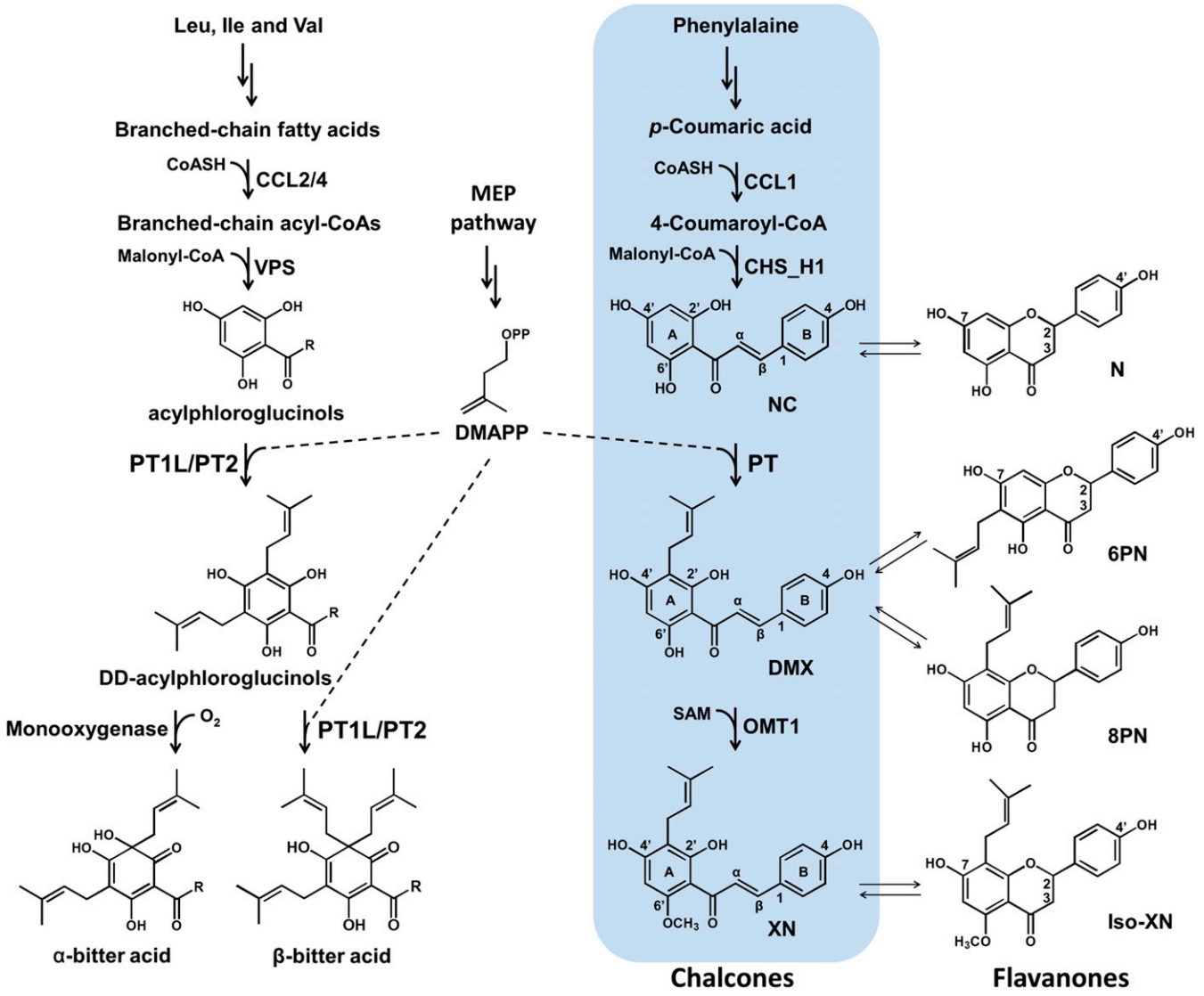

Fig. 1. The proposed biosynthetic pathway for terpenophenolics in hop glandular trichomes. The XN pathway, starting from phenylalanine, is boxed in blue. The possible R-groups in bitter acids are isobutyryl, isopropyl, and butan-2-yl groups. DD-acylphloroglucinols, di-dimethylallylated acylphloroglucinol; Iso-XN, isoxanthohumol; MEP pathway, plastid-localized methylerythritol phosphate pathway; OMT, *O*-methyltransferase; VPS, valerophenone synthase.

gene, *CHS_H1*, has been identified from hops (24). NC is then prenylated by HlPT1L, and further methylated by an *O*-methyltransferase (HlOMT1) to form XN (20, 23, 25). Paradoxically, previous transcriptome data had indicated that several chalcone isomerase (CHI; EC 5.5.1.6) genes represent the most abundant ESTs from hop glandular trichomes that accumulate massive amounts of chalcone (1, 21). While bona fide CHI enzymes were the first to be identified in the context of plant flavonoid metabolism, CHI-fold family proteins are more widespread in other domains of life, such as fungi and bacteria (26). The plant CHI family can be classified into four subfamilies (type I to type IV) according to their phylogenetic relationships. Types I and II CHIs are bona fide catalysts having CHI enzymatic activity. Type I CHIs widely exist in vascular plants and are responsible for the production of plant flavonoids (27–29). Type II CHI proteins appear to be legume-specific and are involved in isoflavonoid production (27, 30). Type III CHIs are widely present in land plants and green algae, while type IV CHIs are restricted to land plants. Structural analysis showed that all CHIs share a similar backbone conformation (25, 30). However, type III and type IV CHIs do not possess bona fide CHI activity, which led to the renaming of both types of CHIs as CHI-like proteins (CHIL). Recently, type III CHI folds from *Arabidopsis* were shown to bind fatty acids in vitro, and play a role in fatty acid metabolism *in planta* (25). Type III CHIs are thus divided into three fatty-acid binding protein subfamilies (FAP1, FAP2, and FAP3). A loss-of-function mutation in type IV CHI from Japanese morning glory (*Ipomoea nil*) led to low amounts of anthocyanin, although the underlying mechanism remains unknown (31). Previous phylogeny and sequence analyses suggest that bona fide CHIs are diverged from type IV CHIs, which evolved from the common ancestor FAP3 (type III CHIs). However, the role of type IV CHIs in flavonoid biosynthesis during land plant evolution remains to be determined (25, 32, 33).

Here, we used *DD104* yeast strain to characterize two hop *CHIL* genes (*HlCHIL1* and *HlCHIL2*). We demonstrate that although lacking CHI activity, both CHILs play a critical role in demethylxanthohumol (DMX)/XN production. HlCHIL2 enhanced the activities of CHS_H1 and PT1L through direct protein–protein interactions, suggesting that a functional metabolon composed of CHS,

CHIL2, and PT1L, directs efficient production of prenylchalcones in hop glandular trichomes. On the other hand, CHIL1 appears to bind and stabilize the ring-open configuration of chalcones during XN biosynthesis. Our study not only reveals the functions of noncatalytic CHIs in flavonoid biosynthesis and the evolutionary trajectory of noncatalytic CHIs in land plants, but also provides valuable insight into engineering heterologous systems to produce high-valued prenylchalcones at a large scale.

Results

Characterization of Two *CHIL* Genes from Hop Glandular Trichomes. We have previously demonstrated that XN biosynthesis occurs predominantly in the glandular trichomes of female hop flowers (1, 21–23). Searching the hop trichome-specific EST library led us to find 260 ESTs representing CHI genes, which were among the most abundant unigenes in the library. Two ORFs of CHIL genes were isolated and designated as *HlCHIL1* and *HlCHIL2*, which encode polypeptides of 214 and 209 amino acids, respectively. HlCHIL1 shares 31% identity to FAP1 (At3g63170) from *Arabidopsis thaliana* (25) and 69% identity to a homologous protein from *Cannabis sativa* (GenBank accession no. JN679226), which is functionally uncharacterized to date (34). HlCHIL2 shares 69.7% identity to AtCHIL (At5g05270), which functions with bona fide CHI (At3g55120) to promote flavonoid production in *Arabidopsis* (35). A maximum-likelihood phylogenetic tree of plant CHIs was constructed to analyze the evolutionary relationship among plant CHIs: CHIL1 belonged to the type III subfamily (FAP1 clade), whereas CHIL2 falls into the type IV subfamily (Fig. 2*A*). Sequence alignments showed that the conserved active residues in bona fide CHI sequences are missing in HlCHIL1 and HlCHIL2, suggesting both are noncatalytic CHIs (*SI Appendix*, Fig. S1). Biochemical assays, using NC and isoliquiritigenin as substrates, at pH 6.4 and 7.5, supported this hypothesis: both CHIL1 and CHIL2 recombinant proteins did not exhibit CHI activity in vitro (*SI Appendix*, Fig. S2). This result is consistent with the fact that prenylchalcones, rather than prenylflavanones, are predominantly accumulated in hop trichomes (21, 22). Quantitative RT-PCR analysis showed that expression of both *HlCHIL1* and *HlCHIL2* was trichome-specific (Fig. 2*B*). Subcellular localization experiments indicated that CHIL1 and CHIL2 were localized to the cytoplasm, where the CCL1, CHS_H1, and OMT1 enzymes of XN biosynthesis are also located (Fig. 2*C*). These results suggested that *CHIL1* and *CHIL2* are likely involved in XN biosynthesis.

CHIL1 and CHIL2 Exert Contrasting Effects on DMX Production. To explore the roles of *HlCHILs* in DMX biosynthesis, we initially reconstructed the DMX pathway by coexpressing *CCL1*, *CHS_H1*, and *PT1L* (*PT* genes used in this study were *Arabidopsis* codon-optimized sequences) in the DD104 yeast strain (23). On feeding with 0.5 mM *p*-coumarate, the engineered strain harboring *CCL1*/*CHS_H1*/*PT1L* was able to produce DMX, whereas the strain harboring *CCL1*/*CHS_H1*/*PT2* could not produce DMX (*SI Appendix*, Fig. S3). Moreover, addition of *PT2* to the *CCL1*/*CHS_H1*/*PT1L* yeast strain did not further improve DMX production (*SI Appendix*, Fig. S3). These results indicated that *HlPT1L* alone is responsible for the prenylation step in the DMX pathway (*SI Appendix*, Fig. S3*B*). Because DMX is converted to 6PN (6-prenylnaringenin) and 8PN (8-prenylnaringenin) in this yeast system, we report total prenylated chalcone/flavanone (DMX, 6PN, and 8PN). When we further introduced *CHIL2* in the DD104 yeast strain harboring *CCL1*/*CHS_H1*/*PT1L*, the *CCL1*/*CHS_H1*/*PT1L*/*CHIL2* strain produced approximate 2.3-fold higher total DMX (4.59 ± 0.98 μmol/L/OD; $n = 3$) than *CCL1*/*CHS_H1*/*PT1L* (2.0 ± 0.31 μmol/L/OD; $n = 3$). Introduction of CHIL2 also increased naringenin (N)/NC production by 1.3-fold (43.97 ± 5.8 μmol/L/OD vs. 34 ± 3.06 μmol/L/OD; $n = 3$) (Fig. 3). Unexpectedly, introduction of CHIL1 to the *CCL1*/*CHS_H1*/*PT1L* strain significantly reduced total DMX production by 30% (1.38 ± 0.32 μmol/L/OD; $n = 3$) (Fig. 3). We also checked the maximal production of N/NC and total DMX by adding *p*-coumarate to the culture (to final concentration 500 μM) every 24 h (29). The results showed that the DD104 yeast strain harboring *CCL1*/*CHS_H1*/*PT1L*/*CHIL2* produced the N/NC and DMX at a relative flat rate (*SI Appendix*, Fig. S4 *A*–*C*). Additionally, most of the N/NC (72%) was secreted into the culture medium, whereas 90% of the DMX remained inside the yeast cells (*SI Appendix*, Fig. S4*D*).

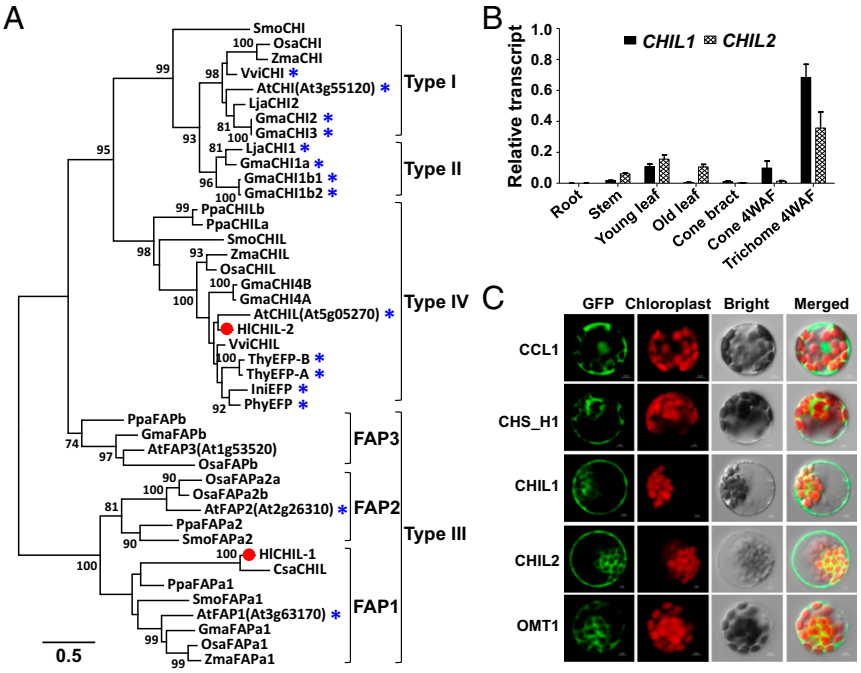

Fig. 2. Characterization of HlCHIL1 and HlCHIL2. (*A*) Phylogenetic analysis of CHI/CHIL proteins from plants using the maximum-likelihood method. A total of 43 CHI/CHIL proteins were obtained from 13 species representative of plant evolutionary history. To simplify the classification of CHI/CHIL proteins, four clades (types I to IV) are shown here. Bootstrap values (based on 1,000 replicates) >70% are shown for corresponding nodes. The two hops CHILs are marked with red dots, and functionally identified CHI/CHILs are marked with blue asterisks. Species abbreviations: At, *Arabidopsis thaliana*; Csa, *Cannabis sativa*; Gma, *Glycine max*; Hl, *Humulus lupulus*; Ini, *Ipomoea nil*; Lja, *Lotus japonicus*; Osa, *Oryza sativa*; Phy, *Petunia hybrida*; Ppa, *Physcomitrella patens*; Smo, *Selaginella moellendorffii*; Thy, *Torenia hybrida*; Vvi, *Vitis vinifera*; Zma, *Zea mays*. Protein sequences used in this analysis are listed in Dataset S1. (*B*) Quantitative RT-PCR analysis of two *CHIL* genes in different tissues of hop plants. Transcript levels are expressed relative to *GADPH* transcripts ($n = 3$). Cone bract, the glandular trichomes were removed; WAF, weeks after flowering. (*C*) Subcellular localization of XN-related enzymes in *Arabidopsis* leaf mesophyll protoplasts as revealed by laser confocal microscopy. Chloroplasts are revealed by red chlorophyll autofluorescence. (Scale bars, 5 μm.)

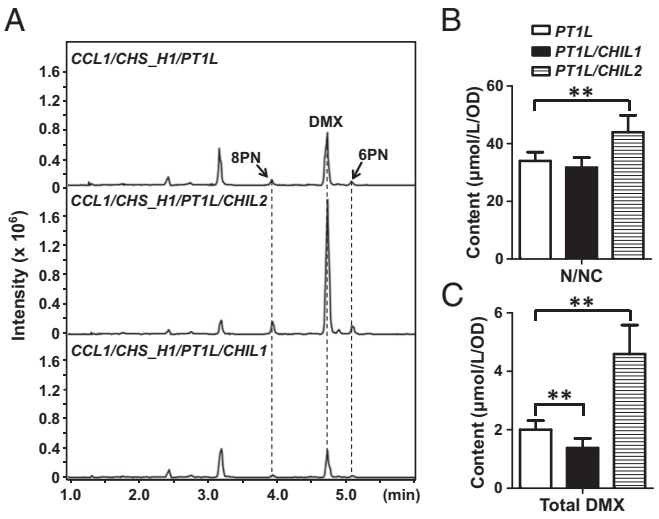

Fig. 3. Effects of *HlCHIL1* and *HlCHIL2* on the production of NC and total DMX in engineered yeasts. (*A*) Chromatogram of selected ions of *m/z* 341.1384 for DMX/8PN/6PN using LC-qTOF-MS. Yeast strains harboring different gene combinations were grown in induction medium for 96 h before chemical extraction and analysis. PT1L used in this experiment was the *Arabidopsis* codon-optimized sequence. (*B*) Production of N/NC by yeast strains harboring no *CHIL* gene (control), *CHIL1*, and *CHIL2*. Data are means ± SD for at least three independent clones (*t* test, $^{**}P < 0.01$). (*C*) Production of DMX/8PN/6PN by yeast strains harboring no *CHIL* gene (control), *CHIL1* or *CHIL2*. Data are means ± SD for at least three independent clones (*t* test, $^{**}P < 0.01$).

Type IV CHI-Folds Physically Interact with Plant CHSs to Enhance CHS Activity. The enhancing effect of CHIL2 on NC and DMX production leads to an assumption that CHIL2 might be physically interacting with other enzymes in the XN pathway. To test this hypothesis, we used the yeast two-hybrid (Y2H) technique to probe for interactions between CHIL2 and other enzymes in the XN pathway. The results showed that CHIL2 interact with CHS_H1, but not with other proteins in the XN pathway (Fig. 4*A*). We further confirmed the interaction between CHIL2 and CHS_H1 using luciferase complementation imaging (Fig. 4*B*) and coimmunoprecipitation (Co-IP) (Fig. 4*C*). As HlPT1L is a membrane-bound protein, we used a split-ubiquitin MbY2H to test for possible interaction between CHIL2 and PT1L, and the results revealed that CHIL2 also physically interacted with PT1L protein (Fig. 4*D*). Furthermore, LUC activity detected in *Nicotiana benthamiana* leaves confirmed the interaction between PT1L and CHIL2 (Fig. 4*E*). We did not find any interaction between CHIL1 and CHIL2, PT1L, CCL1, CHS_H1, or OMT1 (Fig. 4 *A* and *D* and *SI Appendix*, Fig. S5). We further evaluated the influence of CHIL2 on the enzymatic efficiency of CHS_H1 and PT1L through in vitro biochemical analysis. The combination of CHS_H1/CHIL2 had 1.5-fold higher NC production than CHS_H1 alone (*SI Appendix*, Fig. S6*A*). Microsomes prepared from yeast harboring *CHS_H1*/*PT1L*/*CHIL2* displayed 1.4-fold higher DMX production than from yeast harboring only CHS_H1/PT1L (*SI Appendix*, Fig. S6*B*). The conversion rates of purified recombinant CHS_H1 (V_{max} value) were increased by ∼5.6-fold and 17.5-fold with CHIL2 for *p*-coumaroyl-CoA and malonyl-CoA, respectively, although the K_m value also increased by fivefold (Table 1). PT1L/CHIL2 had both a higher conversion rate and a lower K_m value than PT1L alone for both NC and DMAPP (Table 2).

Given that stress-protective flavonoids, type IV CHIs, and CHSs are widely distributed in land plants (25, 36, 37), we assume that type IV CHIs share the conserved function of increasing flavonoid production by binding and increasing the enzymatic efficiency of plant CHSs. To test this hypothesis, we probed the possible type IV CHI–CHS interactions in four plant species [*Physcomitrella patens* (Bryophytes), *Selaginella moellendorffii* (Lycophytes), *Oryza sativa* (monocots in Euphyllophytes), and *Arabidopsis thaliana* (dicots in Euphyllophytes)], which are located at the major nodes during plant evolution. The physical interactions were detected for all six tested type IV CHI–CHS pairs (there are two type IV CHIL genes in the *P. patens* and *O. sativa* genomes) (Fig. 4*F*). All tested type IV CHI proteins enhanced the CHS activity by 1.5- to 3-fold, as indicated by N/NC production in the engineered yeast system (Fig. 4*G*).

To test the function of CHIL2 *in planta*, we also generated transgenic *Arabidopsis* plants overexpressing *CHIL2*, *PT1L*, and *CHIL2-PT1L* in the *tt5-1* background [*TT5* (*At3g55120*), lacking a functional CHI protein; *Ler* ecotype], which accumulates approximate 60-fold more NC compared with *Ler* wild-type (*SI Appendix*, Fig. S7*A*). LC-MS analysis showed that the NC content was increased in *CHIL2* overexpression lines by about 1.6-fold (*SI Appendix*, Fig. S7 *B* and *C*), indicating that CHIL2 increased CHS activity *in planta*. This result drove us to test whether HlCHIL2 physically interacted with the CHS from *A. thaliana* (At5g13930) and other above-mentioned plant CHSs. We found direct interactions between HlCHIL2 and all tested CHS proteins from *P. patens*, *S. moellendorffii*, *O. sativa*, and *A. thaliana* (*SI Appendix*, Fig. S7*D*). However, we were unable to detect DMX or prenylated flavonoids in *PT1L* or *CHIL2-PT1L* overexpressing *Arabidopsis* lines, despite the detection of *PT1L* mRNA in these transgenic plants (*SI Appendix*, Fig. S8).

CHIL1 Binds to DMX and NC to Stabilize the Chalconoids' Ring-Opened Structure. Because CHIL1 significantly reduced DMX production in engineered yeast cells (Fig. 3), although no physical interaction between CHIL1 and other XN-related proteins could be detected (*SI Appendix*, Fig. S5), it is possible that CHIL1 protein binds to DMX, similar to the way that AtFAPs bind with fatty acids in *A. thaliana* (25), and that the bound DMX cannot be released from this metabolite–protein complex by the extraction method used here. To test this hypothesis, we incubated purified His-tagged CHIL1 with the chemical extract (DMX/6PN/8PN) prepared from yeast harboring *CCL1*/*CHS_H1*/*CHI2*/*PT1L*. Most of the DMX was eventually converted to 6PN and 8PN after incubation with His-tagged proteins for 8-h at 4 °C (see *SI Appendix*, Fig. S9 for the experimental workflow). However, CHIL1 protein enriched DMX levels by 14.2-fold [the ratio of (DMX)/(total DMX) in CHIL1-bound chemical mixture was 19.7%; $n = 3$, whereas the ratio of (DMX)/(total DMX) in solution was only 1.39%] (Fig. 5*A*). In contrast, no CHIL2-associated DMX or 8PN were detected under the same incubation conditions, and the MagneHis Ni-Beads showed weak nonspecific binding activity to 6PN only (Fig. 5 *A* and *B*). Differential scanning fluorimetry assays (38) using purified HlCHIL1 protein and standard chemicals further showed that CHIL1 protein binds DMX and NC with K_d (dissociation constant) values of 25.08 μM ($n = 3$) and 43.56 μM ($n = 3$), respectively (Fig. 5 *C* and *D*), whereas no such binding could be detected with N, 6PN, 8PN, or XN. We therefore conclude that the 6PN and 8PN detected in CHIL1-bound compounds are most likely converted from DMX during sample preparation given the known spontaneous isomerization of DMX in vitro. CHIL1 protein showed weaker binding activity to lauric acid (C12:0) and myristic acid (C14:0), than to longer-chain fatty acids (C16:0, C18:0, and C18:3) (*SI Appendix*, Fig. S10). It should be noted that both DMX ($\Delta Tm_{max} = 10.23$ °C, $n = 3$) and NC ($\Delta Tm_{max} = 6.40$ °C, $n = 3$) show a stronger stabilizing effect on CHIL1 protein than do lauric acid ($\Delta Tm_{max} = 5.0$ °C, $n = 2$) or myristic acid ($\Delta Tm_{max} = 3.55$ °C, $n = 2$). However, CHIL1 preferentially binds lauric acid ($K_d = 11.81$ μM, $n = 2$) and myristic acid ($K_d = 3.45$ μM, $n = 2$) compared with DMX ($K_d = 25.08$ μM,

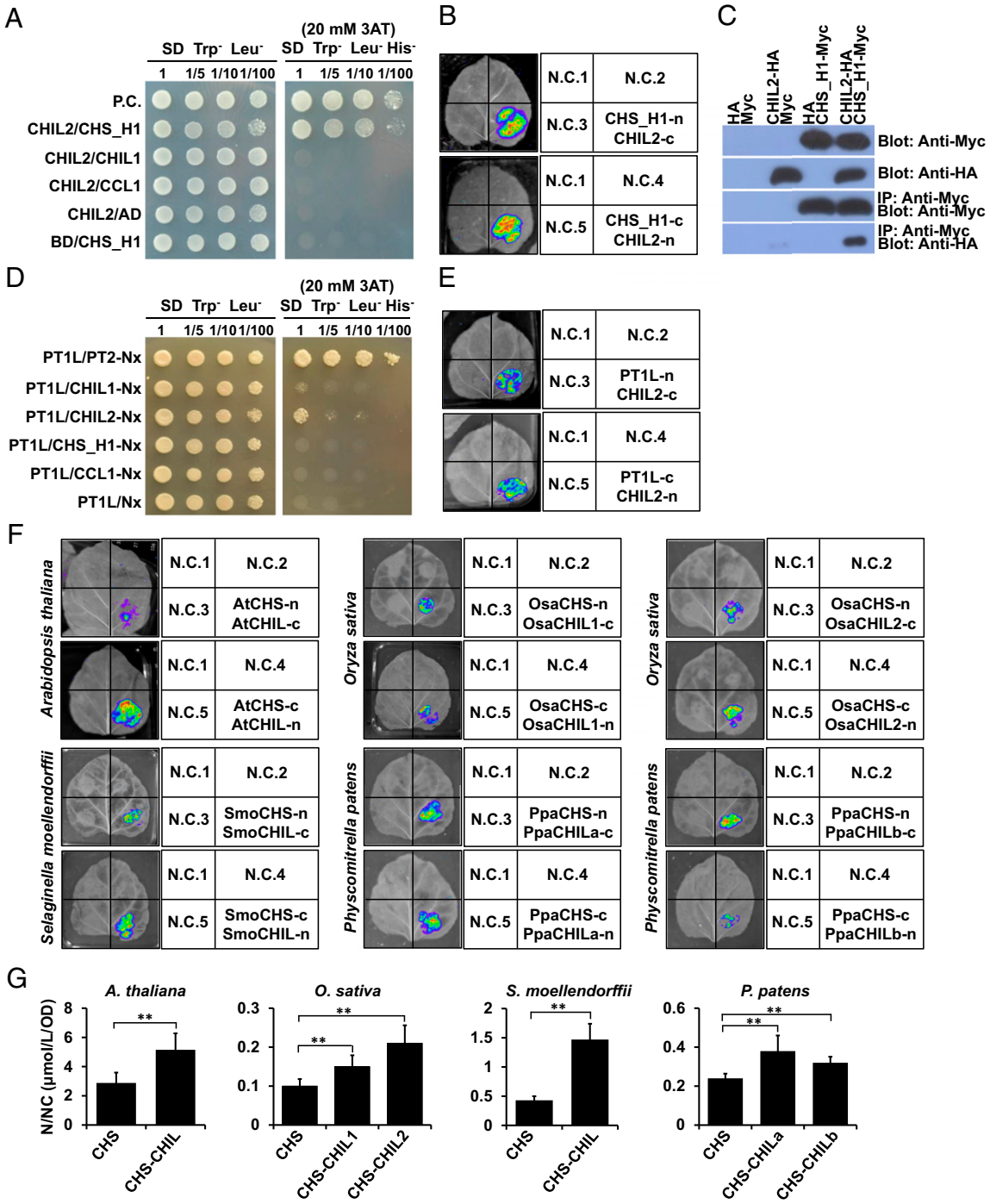

Fig. 4. Direct interactions between type IV CHIs and CHS. (*A*) Protein–protein interactions between CHIL2 and CHS_H1, CHIL1, and CCL1 in a Y2H system. The selective medium [SD-Trp-Leu-His containing 20 mM 3-amino-1,2,4-triazole (3AT)] was used for selecting for the interacting proteins. The *CHIL2* gene was inserted into pGBKT7 vector (BD vector), and *CHS_H1*, *CHIL1*, and *CCL1* were inserted into pGADT7 vector (AD vector). P.C., positive control; the pGBKT7-53 and pGADT7-T constructs used as positive controls were provided by the manufacturer. (*B*) Direct interactions between HlCHIL2 and CHS_H1 in *N. benthamiana* leaves. Luciferase image of *N. benthamiana* leaves coinfiltrated with the agrobacteria containing CHS_H1-nLuc and CHIL2-cLuc or CHIL2-nLuc/CHS_H1-cLuc combinations. (*C*) Reciprocal co-IP of MYC-tagged CHS_H1 and HA-tagged CHIL2 in yeast using HA- and Myc- antibodies. Total protein extracts were prepared from transgenic yeast strain harboring *CHS_H1* and *CHIL2*, alone or together. (*D*) Protein–protein interactions between CHIL2 and PT1L in a split-ubiquitin Y2H system. Selection medium consisting of SD-Trp-Leu-His containing 20 mM 3-amino-1,2,4-triazole (3AT) was used for selecting the interactions between the proteins. The PT1L and PT2 constructs were used as positive controls. All PT genes were *Arabidopsis* codon-optimized sequences. (*E*) Direct interactions between HlCHIL2 and HlPT1L in *N. benthamiana* leaves. Luciferase image of *N. benthamiana* leaves coinfiltrated with agrobacteria containing PT1L-nLuc and CHIL2-cLuc or CHIL2-nLuc/PT1L-cLuc combinations. (*F*) Type IV CHIL–CHS interactions in *P. patens* (there are two type IV CHIL genes in the *P. patens* genome), *S. moellendorffii*, *O. sativa* (there are two type IV CHIL genes in *O.sativa* genome), and *A. thaliana*. (*G*) Production of N/NC by yeast strains harboring *CHS* alone or *CHS-CHIL* combination. Yeast strains harboring different gene combinations were grown in induction medium for 48 h before chemical extraction and analysis. Data are means ± SD for at least three independent clones (*t* test, $^{**}P < 0.01$). N.C.1, negative control 1 (nLuc + cLuc); N.C.2, negative control 2 (Gene1-nLuc + cLuc); N.C.3, negative control 3 (nLuc + Gene2-cLuc); N.C.4, negative control 4 (Gene2-nLuc + cLuc); N.C.5, negative control 5 (nLuc + Gene1-cLuc).

Table 1. Kinetic parameters for CHS_H1 and CHS_H1/CHIL2 complex

Complex	Substrate	K_m (μM)	K_{cat} ($s^{-1} \times 10^{-3}$)	K_{cat}/K_m ($M^{-1}s^{-1}$)
CHS_H1	*p*-Coumaroyl-CoA*	4.82 ± 0.99[†]	0.21 ± 0.02	44
	Malonyl-CoA[‡]	10.06 ± 2.99	0.24 ± 0.03	24
CHS_H1/CHIL2	*p*-Coumaroyl-CoA*	26.57 ± 3.78	1.2 ± 0.12	45
	Malonyl-CoA[†]	59.74 ± 8.49	4.2 ± 0.3	70

Two micrograms of purified recombinant CHS_H1 were used in each CHS_H1 assay; and 2 μg of purified recombinant CHS_H1 and 1.1 μg of purified recombinant CHIL2 (CHS_H1:CHIL2 = 1:1) were used in each CHS_H1/Hl CHIL2 assay.
*A fixed concentration of 150 μM malonyl-CoA was used as substrate.
[†]The data are presented as means ± SD (n = 3).
[‡]A fixed concentration of 40 μM *p*-Coumaroyl-CoA was used as substrate.

n = 3) and NC (K_d = 43.56 μM, n = 3) (*SI Appendix*, Fig. S10). These results demonstrate that CHIL1 protein not only binds to DMX and NC, but also stabilizes the ring-open configuration of these compounds.

To further investigate the structural basis for DMX binding, a homology model was generated for HlCHIL1 using AtFAP1 (PDB ID code 4DOO) as a template (25). Subsequent docking simulations for DMX revealed a similar binding pocket compared with lauric acid (C12:0) in the AtFAP1 model (Fig. 5*E*). The best-fitting DMX pose positioned the molecule such that the 4′- and 6′-hydroxyl groups of ring A formed hydrogen bonds with the backbone carbonyl of V139 and the side chain of Y186, respectively, whereas M155 and M196 could be found within reasonable hydrogen bonding distance of the 2′-hydroxyl of ring A and the 4′-hydroxyl of ring B, respectively (Fig. 5*F*). Additional binding interactions are established via π-stacking of F115 with ring A and potential cation–π stabilization via R42 with ring B (Fig. 5*F*). This binding orientation places the Cβ atom of DMX 5.0 Å away from the 2′-hydroxyl, rationalizing both the ability of HlCHIL1 to stabilize the ring-open conformation and the absence of any CHI activity.

CHIL1 and Its Homologs Are Functionally Diverged from FAP1 Proteins. To trace the evolutionary history of HlCHIL1, we identified HlCHIL1 homologs in diverse plant species by BLAST (National Center for Biotechnology Information and Phytozome database, phytozome.jgi.doe.gov/) using 50% identity as cut-off. The comprehensive phylogenetic analysis of the FAP1 subfamily shows that 33 HlCHIL1 homologs form a distinct branch which separated from FAP1 proteins after the emergence of the angiosperms, as no close homologs of HlCHIL1 can be found in ancient species, such as gymnosperms, pteridophytes, and bryophytes (*SI Appendix*, Fig. S10). Interestingly, most AtFAP1 homologs, ranging from bryophytes to flowering plants, show a clear N-terminal plastidial signal peptide (*SI Appendix*, Table S1) (predicted by TargetP software, www.cbs.dtu.dk/services/TargetP/), suggesting that AtFAP1 homologs shared a conserved biochemical function involving fatty-acid metabolism, as demonstrated previously (25). However, all of the closest homologs of HlCHIL1 do not have a clear N-terminal signal peptide. This, together with the biochemical characterization of HlCHIL1 (binding with DMX for structural stabilization), suggests a divergent function of HlCHIL1 homologs from the conserved fatty-acid binding activity of FAP1s.

When comparing the amino acids, which are critical for binding fatty acids in AtFAP1 or DMX in HlCHIL1, most amino acids in the fatty acids binding cleft of FAP1 proteins, including the Arg-Tyr pair that tethers the carboxylate group, are conserved in CHIL1 homologs (Fig. 6*A*). It is noteworthy that Phe203 and Phe207 in AtFAP1 are substituted with Val139 and Ala143 in HlCHIL1, which results in an enlarged binding pocket for accommodating the aromatic ring A of DMX. To test the importance of these two amino acids for DMX binding, we generated V139F and A143F CHIL1 single mutants and V139F/A143F double mutant. Binding assays clearly showed that single CHIL1 mutant ($CHIL1^{V139F}$ and $CHIL1^{A143F}$) had similar binding properties toward DMX (ΔTm_{max} = 10.15 °C and 10.87 °C for $CHIL1^{V139F}$ and $CHIL1^{A143F}$, respectively; n = 3) and NC (ΔTm_{max} and K_d are 5.50 °C and 7.34 °C for $CHIL1^{V139F}$ and $CHIL1^{A143F}$, respectively; n = 2), compared with those of wild-type CHIL1 (ΔTm_{max} = 10.23 °C for DMX and 6.40 °C for NC; n = 3) (Fig. 6*B*). However, both DMX (ΔTm_{max} = 5.26 °C, n = 3) and NC (ΔTm_{max} = 4.70 °C, n = 2) show much weaker stabilizing effect on $CHIL1^{V139F/A143F}$ compared with CHIL1 (Fig. 6*B*), suggesting that V139 and A143 of CHIL1 have a joint effect on DMX/NC binding to CHIL1. It is noteworthy that $CHIL1^{V139F}$ shows higher affinity to DMX (K_d = 10.05 μM) and NC (K_d = 7.61 μM) than CHIL1 (Fig. 6*B*). Altogether, we tentatively designate these HlCHIL1 homologs as polyketide (a term covering flavonoid) binding proteins (PBP).

Discussion

It is well-known that flavonoids are ubiquitously present in land plants, where they may have played a key role in land colonization during plant evolution (39). CHS, the first enzyme of the flavonoid biosynthetic pathway, has been intensively studied at the biochemical and molecular levels during past three decades. Recently, a proteolytic regulator (At1g23390, encoding a Kelch domain-containing F-box protein) controlling CHS stability was functionally identified from *A. thaliana* (40). Here, we have identified another regulator of plant CHS, the type IV CHI-fold proteins, which physically interact with CHS to increase its activity, thereby enhancing flavonoid production. This characterization explains the previous observations that loss-of-function of type IV CHI from Japanese morning glory (*I. nil*) and *Arabidopsis* leads to decreased amounts of flavonoids (31, 35). Presumably through protein–protein interactions, the type IV CHI remodels the active-site cavity of CHS for synthesizing NC. The crystal structure of the HlCHIL2/HlCHS_H1 will definitely elucidate the underlying molecular mechanism.

The CHS-enhancing property of the type IV CHI-fold proteins is conserved from mosses to flowering plants (Fig. 4). Although

Table 2. Kinetic parameters for PT1L and PT1L/CHIL2 complex

Complex	Substrate	K_m (μM)	V_{max} (μmol/min/g)	V_{max}/K_m
PT1L	NC*	5.74 ± 0.68[†]	0.1 ± 0.01	0.0174
	DMAPP[‡]	75.12 ± 15.7	0.13 ± 0.02	0.0017
PT1L/CHIL2	NC*	5.01 ± 0.43	0.12 ± 0.01	0.024
	DMAPP[‡]	62.78 ± 6.76	0.23 ± 0.01	0.0037

Total membrane-bound proteins (10 μg in each assay) were prepared from the yeast harboring *PT1L* or *PT1L/CHIL2*.
*A fixed concentration of 50 μM DMAPP was used as substrate.
[†]The data are presented as means ± SD (n = 3).
[‡]A fixed concentration of 200 μM NC was used as substrate.

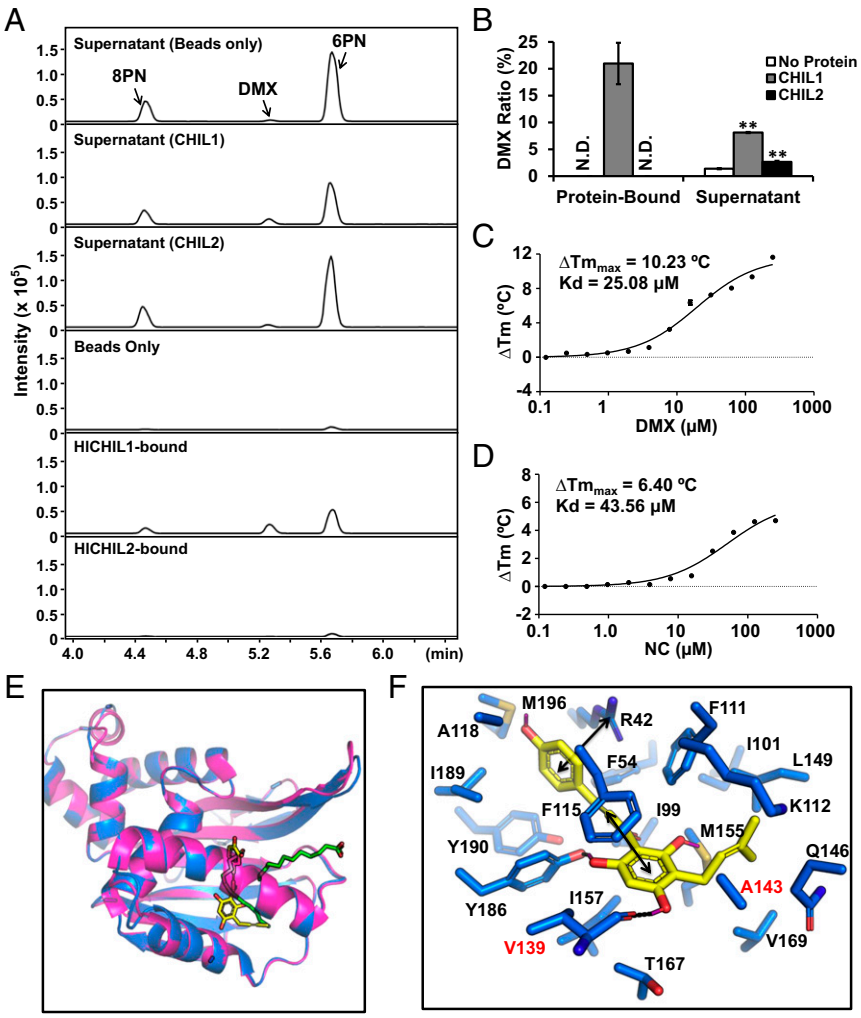

Fig. 5. Identification of DMX binding of CHIL1. (*A*) Analysis of ligands associated with purified His-tagged HlCHIL1 protein (linked to MagneHis Ni-Particles) separated and detected by LC-QQQ-MS/MS (MRM condition for DMX/6PN/8PN: 341.0 → 165.0). MagneHis Ni-Beads alone were used as negative controls in these assays. All samples, including the chemical extract only, were incubated at 4 °C for 8 h before LC-MS analysis (for details, see *SI Appendix*, Fig. S9). (*B*) Relative quantification of DMX in protein-bound and supernatant fractions of different CHIL–small-molecule interaction assays. N.D., not determined due to low content of DMX in the samples (*t* test, $^{**}P < 0.01$). (*C*) Representative dose–response curves for HlCHI1 generated using thermal shift response to increasing DMX concentration. ΔTm_{max} and K_d values were calculated as 10.23 °C and 25.08 μM, respectively ($n = 3$). (*D*) Representative dose–response curve for HlCHIL1 generated using thermal shift response to increasing NC concentration. ΔTm_{max} and K_d values were calculated as 6.40 °C and 43.56 μM, respectively ($n = 3$). (*E*) Homology model of HlCHIL1 (marine) with docked DMX ligand (yellow sticks) overlaid with AtFAP1 (PDB ID code 4DOO; magenta) bound to lauric acid (green sticks). The homology model was built using AtFAP1 as a template. (*F*) Zoomed-in view of HlCHIL1 with docked DMX, showing relevant protein side chains as gray sticks. Selective hydrogen atoms are shown in purple, H-bonding interactions as dotted black lines, and potential π-stacking or cation–π stabilization interactions as solid black arrows. Val139 and Ala143 are highlighted in red due to their important role in DMX binding.

phylogenetic analysis suggested that the type IV CHI-fold proteins were probably the ancestor of plant functional CHIs, the function of type IV CHI-fold proteins remained unknown (25, 32, 33). Based on our data, we propose that binding with CHS is a conserved function for all plant CHI-fold proteins, type I and type II CHI-fold proteins inherited this trait from type IV CHI-fold proteins besides the gained CHI activity during enzyme evolution. The physical interaction between bona fide CHI and CHS has been demonstrated in plants (41). Given the importance of flavonoids, enhancing CHS activity likely enhances plant fitness. Phylogenetic analysis also shows that type IV CHIs are likely derived from FAP3 proteins, which are involved in fatty acid metabolism in plants. Therefore, it will be worth testing whether plant FAP3 proteins physically interact with enzymes of fatty acid biosynthesis, especially the ketoacyl-[acyl-carrier-protein] synthase III, which is the progenitor of plant CHSs (42).

HlCHIL2 physically interacts with PT1L to form an active metabolon for DMX production in hop glandular trichomes. PT1L, as a membrane-bound protein, therefore functions to anchor the complex with CHIL2, which also interacts with CHS_H1, to the membrane. In *Arabidopsis*, a type IV CHI-fold protein (AtCHIL, At5g05270) was demonstrated to bind with bona fide CHI protein (type I CHI, At3g55120) for flavonoid production (35). These results suggest that type IV CHI-fold proteins may bind with enzymes downstream of CHS in a species-dependent manner; this needs to be experimentally validated.

Meanwhile, CHIL1 binds and stabilizes the ring-open conformation of NC and DMX, the intermediates of XN biosynthesis. The DMX-binding ability of CHIL1 and the DMX metabolon presented here are consistent with the chemical phenomenon observed in hop glandular trichomes: high accumulation of DMX and XN, with almost no N/NC being detected

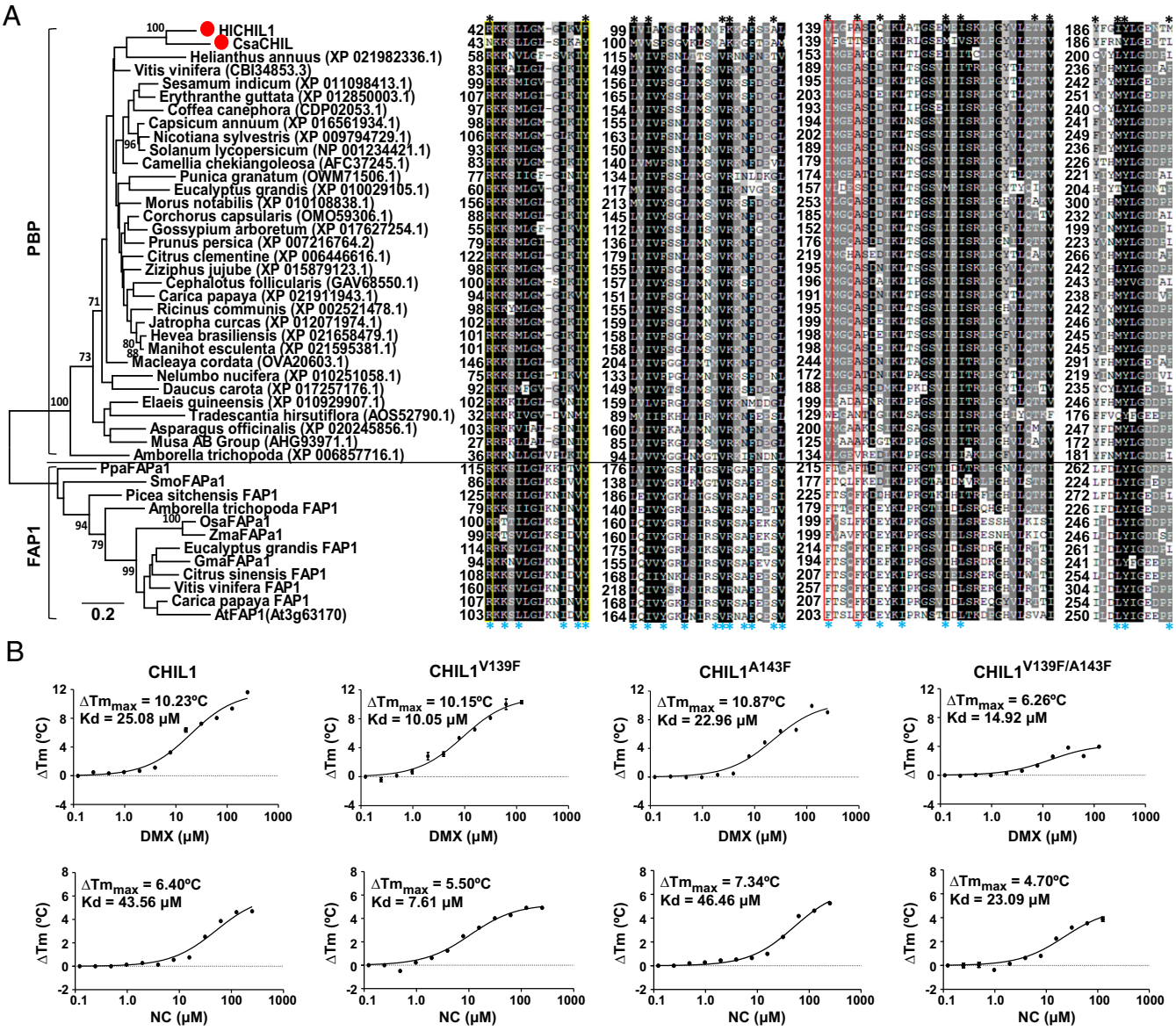

Fig. 6. Sequence analysis of HlCHIL1 homologs and chemical binding identification of CHIL1 mutants. (*A*) Thirty-three HlCHIL1-close proteins (>50% identity) were added for the phylogenetic analysis. The GenBank number for each HlCHIL1-close protein is provided in parenthesis, next to the Latin name of the plant species. Bootstrap values (based on 1,000 replicates) >70% are shown for corresponding nodes. HlCHIL1 and CsaCHIL are marked in red dots. Twenty residues lining the DMX binding site, based on the HlCHIL1 modeling information, are denoted by red asterisks. Twenty-six residues lining the fatty-acid binding site, based on the AtFAP1 structure information, are denoted by blue asterisks. The Arg-Tyr pair (R103 and Y116 in AtFAP1) that tethers the carboxylate group in FAP1s and the Val139 and Ala143 that are critical for accommodation of DMX in HlCHIL1 are boxed in yellow and red, respectively. For species abbreviations, see the legend to Fig. 1*A*. Protein sequences used in this analysis are listed in Dataset S2. (*B*) Representative dose–response curve for CHIL1, CHIL1^{V139F}, CHIL1^{A143F}, and CHIL1$^{V139F/A143F}$ generated using thermal shift response to increasing DMX or NC concentration.

(21, 22). The structural information and sequence analysis has led to the discovery of a protein clade (PBP) with unprecedented functions: HlCHIL1 homologs probably bind with the products of other type III polyketide synthases, at least those that contain an aromatic ring derived from the condensation of three molecules of malonyl CoA (Fig. 5). CsaCHIL (from *C. sativa*, Cannabaceae) is the closest homolog of HlCHIL1 (69% identity), and is specifically expressed in hemp glandular trichomes (34). Two polyketides, Δ^9-tetrahydrocannabinolic acid (THCA) and cannabidiolic acid (CBDA), are synthesized and stored at high levels in hemp glandular trichomes. THCA and CBDA, like DMX, are unstable and will be nonenzymatically converted to the decarboxylated forms, Δ^9-tetrahydrocannabinol and cannabidiol, respectively. We therefore hypothesize that CsaCHIL probably binds with THCA and/or CBDA to stabilize these compounds in hemp glandular trichomes. Furthermore, the endogenous content of free polyketides will be accordingly decreased due to increased protein-bound forms, which can alleviate the feedback inhibition of polyketide biosynthesis to result in high production of polyketides in a specific plant cell/tissue/organ.

In conclusion, we have functionally identified two CHIL genes, *HlCHIL1* and *HlCHIL2*, which play a significant role in DMX biosynthesis in hop glandular trichomes: CHIL2 enhances the catalytic efficiency of CHS_H1 and PT1L through protein–protein interactions, whereas CHIL1 stabilizes the ring-open conformation of DMX. Moreover, the engineered yeast generated in this study produced up to 4.59 μmol/L/OD of DMX

under flask-shake conditions, which will be a starting point for producing these valuable prenylchalcones at large scale using microbial cell factories.

Materials and Methods

Plant Materials, RNA Analysis, and Chemicals. The growth of *H. lupulus* cv. Nugget, EST sequence analysis, RNA isolation, and cDNA preparation from hop tissues were performed as described previously (1). *A. thaliana* (Col-0 ecotype) and *N. benthamiana* plants for transient transformation were maintained in a greenhouse under 16-h light/8-h dark, 22 °C conditions. All available commercial chemicals used in this study were purchased from Sigma-Aldrich, except for NC, which was purchased from ChromaDex. PIVP (phlorisovalerophenone) was synthesized as described previously (43). The purity and concentration of these chemicals were determined using LC-MS.

Hop CHI Gene Isolation. To obtain the full-length sequences of *HlCHIL1* and *HlCHIL2* from hop trichomes, the ORFs of *HlCHIL1* and *HlCHIL2* obtained by RT-PCR were cloned into pEASY-Blunt vector (TransGen Biotech) and verified by sequencing of at least five independent clones (see *SI Appendix*, Table S2 for primer information).

Quantitative RT-PCR Analysis. Real-time PCR analyses were performed using Ultra SYBR Mixture (CWBio) on a CFX96 Real-Time PCR Detection System (Bio-Rad) following the manufacturer's instructions. Ct values were calculated using the Bio-Rad real-time analysis software. Comparative Ct method was used for relative gene expression analysis by normalizing to the reference gene [*glyceraldehyde-3-P dehydrogenase* (*GAPDH*) from hop and *Actin2* (*At3g18780*) from *Arabidopsis*]. Every PCR was repeated with three independent biological replicates. Primers are listed in *SI Appendix*, Table S2. All raw real-time PCR analysis data are showed in Dataset S3.

Subcellular Localization. The ORF of the hGFP gene was fused to the C-terminal of the *CCL1*, *CHS_H1*, *CHIL2*, *CHIL1*, and *OMT1* ORFs, under control of the CaMV 35S promoter (pJIT163-hGFP vector). *Arabidopsis* leaf protoplast preparation, transformation, and image assay using laser scanning confocal microscopy were performed as described previously (44). Briefly, mesophyll protoplasts freshly isolated from rosette leaves of 4-wk-old *Arabidopsis* (Col-0 ecotype). The fresh prepared protoplasts are transfected with 10 μg plasmid using a PEG-calcium–mediated transfection method. Living cellular image of GFP fusion proteins are observed under Axio Imager Z2 fluorescence microscopy (Zeiss). Localization was determined by surveying more than 50 protoplasts. Primers are listed in *SI Appendix*, Table S2.

Reconstitution of DMX Pathway in Yeast and Product Analysis. The following vectors were used: pESC-Leu for *CCL1* and *CHIL2*, pESC-His for *CHS_H1* and *CHIL1*, and pESC-Ura for *PT1L* and *PT2*. The different combinations of three constructs (either empty vector or the construct with inserts) were cotransformed into yeast strain DD104 using a high-efficiency lithium acetate transformation protocol (45). The resulting positive yeast clones were cultured in SD dropout medium (-Leu, -His, -Ura), and then harvested and induced with 2% galactose dropout medium (-Leu, -His, -Ura) for 4 d, then fed with 500 μM *p*-coumarate. Chemical extraction and LC-MS analysis were performed as previously described (22, 23). PIVP (1.5 μM) was added as internal standard. The contents of N/NC and DMX/6PN/8PN in the samples were quantified based on the concentration of the internal standard after normalization.

In Vitro Enzyme Assays. Yeast microsome preparations were made as described previously (46). The soluble and microsomal proteins were used directly for enzymatic assays after quantification of protein by Bradford assay. The chalcone synthase assay reaction contained 50 mM Tris·HCl (pH 7), 0.1 mg/mL BSA, 30 μM malonyl-CoA, 10 μM *p*-coumaroyl-CoA, and 40 μg total soluble proteins. The reaction mixtures were incubated in a total volume of 200 μL at 30 °C for 60 min. The PT assays were performed as previously described (23). Control reactions were performed with boiled protein. For the determination of apparent K_m values for different substrates, 40 μM *p*-coumaroyl-CoA was added in the standard CHS_H1 reactions (200 μL volume) containing 2 μg purified recombinant CHS_H1, with or without 1.1 μg of purified recombinant CHIL2 (CHS_H1:CHIL2 = 1:1), and malonyl-CoA at a series of concentrations, or 150 μM malonyl-CoA was added in the standard CHS_H1 reactions containing 2 μg purified recombinant CHS_H1, with or without 1.1 μg of purified recombinant CHIL2 (CHS_H1:CHIL2 = 1:1), and *p*-coumaroyl-CoA at a series of concentrations. DMAPP (50 μM) was added in the standard PT reactions (200 μL) containing 10-μg membrane proteins and NC at a series of concentrations, or 200 μM NC was added in the standard PT reactions containing 10-μg membrane proteins and DMAPP at a series of concentrations. The enzymatic products were extracted and quantified as previously described (23). The apparent K_m data were calculated using Hanes plots (Hyper32, v1.0.0).

CHI assays were carried out as described previously (27, 47), using NC and isoliquiritigenin as substrates, at pH 6.4 and 7.5. Two microliters of each enzymatic reaction, after filtered through a 0.22-μm syringe filter, was loaded on a 1290 Infinity LC pump coupled to a 6495 triple quadrupole mass spectrometer equipped with a dual electrospray ion source operated in positive mode (LC-QQQ-MS/MS; Agilent). Chromatographic separation was performed on a ZORBAX Extend C18 column (50 mm × 2.1 mm ID, 1.8 μm; Agilent). Gradient condition of the mobile phase (solution A is water and solution B is methanol; flow rate is 0.35 mL/min) was set as follows: 0–6 min, a linear gradient of from 40% of B to 60% of B; 6.0–6.5 min, a linear gradient of from 60% of B to 98% of B; 6.5–7.5 min, 98% of B; then the system was equilibrated using the initial condition (40% of B) for 5 min before the next sample injection.

Yeast Two-Hybrid Assays. Yeast two-hybrid assays were based on the Matchmaker GAL4 two-hybrid system (Clontech). *CHIL2* was inserted into pGBKT7 vector, and *CCL1*, *CHS_H1*, *CHIL1* were inserted into pGADT7 vector. Constructs were cotransformed into the yeast strain AH109. The presence of the transgenes was confirmed by growth on SD/-Leu/-Trp plates. To assess protein interactions, the transformed yeast was suspended in liquid SD/-Leu/-Trp medium and cultured to OD_{600} = 1.0. Ten microliters of suspended yeast was spread on SD/-His/-Leu/-Trp medium with 20 mM 3-AT. Interactions were observed after 3 d of incubation at 30 °C. The split-ubiquitin MbYTH assays were performed with a DUAL membrane kit following the manufacturer's instructions (Dualsystems Biotech). *PT1L* was cloned into the bait vector pTMBV4, and *CHIL1*, *CHIL2*, CHS_*H1*, and *CCL1* were cloned into the pDL2-Nx vector. Constructs were cotransformed into the yeast strain DSY-1. The experiments were repeated for at least three times. The primers used in this study are listed in *SI Appendix*, Table S2.

Luciferase Complementation Imaging Assay. *CHIL* genes (*AtCHIL*, *OsCHIL1*, *OsCHIL2*, *SmCHIL*, *PpCHILa*, and *PpCHILb*), *PT1L*, and *CHS* genes (*CHS_H1*, *AtCHS*, *OsCHS*, *SmCHS* and *PpCHS*) were fused to the N- or C-terminal part of LUC to generate the corresponding nLUC and cLUC constructs. *Agrobacterium tumefaciens* GV3101 containing the corresponding n-LUC and c-LUC fusion constructs were simply mixed with P19, then infiltrated into leaves of *N. benthamiana* for transient expression. LUC activity was detected after 48–72 h. The luciferase complementation imaging assays were performed as previously described (48), using three biological replicates, by infiltration of leaves on separate plants. Primers used for the vector construction are shown in *SI Appendix*, Table S2.

Co-IP Assays. N-terminal HA-tagged CHIL2 and Myc-tagged CHS_H1 were cloned into the pESC-Trp and pESC-HIS vectors respectively. HA-pESC-Trp and Myc-pESC-HIS plasmids which expressed HA tag or Myc tag alone were constructed as negative controls using a PCR-mediated method (for primer information, see *SI Appendix*, Table S2). The transformed yeast cells (DSY-1 strain) were harvested after galactose induction until the OD_{600} value reached 1.0, and disrupted with glass beads with the Mini-Bead-Beater (Biospec Products) in an extraction buffer (2 mL/g cells) containing 50 mM Tris·HCl (pH 7.5), 1 mM EDTA, 1%Triton X-100, 1 mM phenylmethylsulfonyl fluoride, 1 μg/mL leupeptin, and 1 μg/mL pepstatin. Glass beads and cell debris were removed by centrifugation at 12,000 × *g* for 10 min. The supernatant was incubated with the first antibody (anti-Myc) at 4 °C overnight with shaking, followed by incubation with Protein G Agarose beads for an additional 2 h. The beads were washed twice with extraction buffer supplemented with 300 mM NaCl and then the proteins were released by incubation for 10 min in SDS sample buffer at 98 °C and analyzed with immunoblotting using an anti-HA antibody.

Chemical Measurements in the Transgenic *Arabidopsis* Lines. Empty pGreen binary vector (control) (49), CHIL2, PT1L, and CHIL2-PT1L were introduced into *tt5-1* mutant *Arabidopsis* using the floral-dip method (50). Two-week-old seedlings, grown on 1/2 MS plates, were ground into a fine powder in liquid nitrogen, of which 200-mg fresh weight equivalents was extracted with 1.6 mL of ethyl acetate. After centrifugation for 10 min, the supernatant was evaporated to dryness and the residue dissolved in methanol and filtered through a 0.22-μm syringe filter. N/NC measurements were conducted using above-mentioned LC-QQQ-MS/MS program.

Protein–Metabolite Interaction Assay. *CHIL* genes were subcloned into the pEasy-Blunt E2 Expression vector (Transgen). All constructs were transformed into *Escherichia coli* BL21(+) cells for prokaryotic expression, and the resulting His-tagged fusion proteins were purified using Ni-NTA affinity chromatography. Quantification and evaluation of the relative purity of the recombinant proteins was performed using SDS/PAGE with BSA as a standard. The in vitro reaction buffer contained 50 mM Tris·HCl, pH 7.5, 20% methanol, 8 μL yeast extracts (final concentration around 200 μM N/NC, 5 μM DMX), and 30 μg purified protein in a final volume of 500 μL. After incubation at 4 °C for 8 h, the protein in the buffer was extracted using MagneHis Protein Purification System (Promega). The compounds were extracted from the supernatant using ethyl acetate, while the MagneHis Ni-Beads were washed twice with 50 mM Tris·HCl (pH 7.5), and the bound chemicals were eluted with ethyl acetate. The chemicals obtained from the supernatant and Ni-Beads were analyzed by LC-QQQ-MS/MS, as described above.

Differential Scanning Fluorimetry Assays. The parameters (K_d and ΔTm_{max}) of CHIL1 binding with DMX or NC were measured using a StepOne real-time PCR system (Applied Biosystems) as previously described (25, 38). The reaction assays contained 5.0 μL of Protein Thermal Shift Buffer, 2.5 μL of 8× Diluted Protein Thermal Shift Dye, 5 μM purified HlCHIL protein, in a final volume of 20 μL. The chemicals used in these assays were serially diluted from 250 μM to 0.12 μM (total 12 points), and K_d and ΔTm_{max} were calculated using GraphPad Prism 5 from at least three biological replicates.

Homology Modeling and Docking Simulations. All structure modeling was performed using the Maestro software package from Schrödinger LLC. The homology model was generated using Prime with AtFAP1 (PDB ID code 4DOO) as the template model. Hydrogen atoms were added to the model and minimized before docking simulations. Potential binding pockets were identified with SiteMap and the DMX ligand was prepared using LigPrep. Individual DMX docking poses were obtained and scored using Glide, then assessed for selection of the best fit. PyMOL was used for the generation of the final model images.

ACKNOWLEDGMENTS. We thank Dr. Francis Karst (University of Strasbourg) for providing the DD104 yeast strain; and Dr. Jungui Dai (Institute of Materia Medica, Chinese Academy of Medical Sciences and Peking Union Medical College) for providing the demethylxanthohumol standard. This work was financially supported National Natural Sciences Foundation of China Grant 31470387, and the State Key Laboratory of Plant Genomics of China Grants SKLPG2016B-5 and 2016A0219-11 (to G.W.).

1. Wang G, et al. (2008) Terpene biosynthesis in glandular trichomes of hop. *Plant Physiol* 148:1254–1266.
2. Van Cleemput M, et al. (2009) Hop (*Humulus lupulus*)-derived bitter acids as multipotent bioactive compounds. *J Nat Prod* 72:1220–1230.
3. Stevens JF, Page JE (2004) Xanthohumol and related prenylflavonoids from hops and beer: To your good health! *Phytochemistry* 65:1317–1330.
4. Stevens JF, et al. (2000) Prenylflavonoid variation in *Humulus lupulus*: Distribution and taxonomic significance of xanthogalenol and 4′-*O*-methylxanthohumol. *Phytochemistry* 53:759–775.
5. Zanoli P, Zavatti M (2008) Pharmacognostic and pharmacological profile of *Humulus lupulus* L. *J Ethnopharmacol* 116:383–396.
6. Obara K, Mizutani M, Hitomi Y, Yajima H, Kondo K (2009) Isohumulones, the bitter component of beer, improve hyperglycemia and decrease body fat in Japanese subjects with prediabetes. *Clin Nutr* 28:278–284.
7. Saugspier M, et al. (2012) Hop bitter acids exhibit anti-fibrogenic effects on hepatic stellate cells in vitro. *Exp Mol Pathol* 92:222–228.
8. Everard A, Geurts L, Van Roye M, Delzenne NM, Cani PD (2012) Tetrahydro iso-alpha acids from hops improve glucose homeostasis and reduce body weight gain and metabolic endotoxemia in high-fat diet-fed mice. *PLoS One* 7:e33858.
9. Miranda CL, et al. (2000) Antioxidant and prooxidant actions of prenylated and nonprenylated chalcones and flavanones in vitro. *J Agric Food Chem* 48:3876–3884.
10. Gerhäuser C (2005) Beer constituents as potential cancer chemopreventive agents. *Eur J Cancer* 41:1941–1954.
11. Zhuang C, et al. (2017) Chalcone: A privileged structure in medicinal chemistry. *Chem Rev* 117:7762–7810.
12. Yoshimaru T, et al. (2014) Xanthohumol suppresses oestrogen-signalling in breast cancer through the inhibition of BIG3-PHB2 interactions. *Sci Rep* 4:7355.
13. Yong WK, Abd Malek SN (2015) Xanthohumol induces growth inhibition and apoptosis in ca ski human cervical cancer cells. *Evid Based Complement Alternat Med* 2015:921306.
14. Goto K, et al. (2005) Enhanced antitumor activity of xanthohumol, a diacylglycerol acyltransferase inhibitor, under hypoxia. *Cancer Lett* 219:215–222.
15. Rodriguez RJ, Miranda CL, Stevens JF, Deinzer ML, Buhler DR (2001) Influence of prenylated and non-prenylated flavonoids on liver microsomal lipid peroxidation and oxidative injury in rat hepatocytes. *Food Chem Toxicol* 39:437–445.
16. Hartkorn A, et al. (2009) Antioxidant effects of xanthohumol and functional impact on hepatic ischemia-reperfusion injury. *J Nat Prod* 72:1741–1747.
17. Willson CM, Grundmann O (2017) In vitro assays in natural products research—A matter of concentration and relevance to in vivo administration using resveratrol, α-mangostin/γ-mangostin and xanthohumol as examples. *Nat Prod Res* 31:492–506.
18. Dai X, et al. (2010) TrichOME: A comparative omics database for plant trichomes. *Plant Physiol* 152:44–54.
19. Wang G, Dixon RA (2009) Heterodimeric geranyl(geranyl)diphosphate synthase from hop (*Humulus lupulus*) and the evolution of monoterpene biosynthesis. *Proc Natl Acad Sci USA* 106:9914–9919.
20. Tsurumaru Y, et al. (2012) HlPT-1, a membrane-bound prenyltransferase responsible for the biosynthesis of bitter acids in hops. *Biochem Biophys Res Commun* 417: 393–398.
21. Nagel J, et al. (2008) EST analysis of hop glandular trichomes identifies an *O*-methyltransferase that catalyzes the biosynthesis of xanthohumol. *Plant Cell* 20:186–200.
22. Xu H, et al. (2013) Characterization of the formation of branched short-chain fatty acid:CoAs for bitter acid biosynthesis in hop glandular trichomes. *Mol Plant* 6: 1301–1317.
23. Li H, et al. (2015) A heteromeric membrane-bound prenyltransferase complex from hop catalyzes three sequential aromatic prenylations in the bitter acid pathway. *Plant Physiol* 167:650–659.
24. Novák P, Matoušek J, Bříza J (2003) Valerophenone synthase-like chalcone synthase homologues in *Humulus lupulus*. *Biol Plant* 46:375–381.
25. Ngaki MN, et al. (2012) Evolution of the chalcone-isomerase fold from fatty-acid binding to stereospecific catalysis. *Nature* 485:530–533.
26. Gensheimer M, Mushegian A (2004) Chalcone isomerase family and fold: No longer unique to plants. *Protein Sci* 13:540–544.
27. Ralston L, Subramanian S, Matsuno M, Yu O (2005) Partial reconstruction of flavonoid and isoflavonoid biosynthesis in yeast using soybean type I and type II chalcone isomerases. *Plant Physiol* 137:1375–1388.
28. Dixon RA, Blyden ER, Robbins MP, Vantunen AJ, Mol JN (1988) Comparative biochemistry of chalcone isomerases. *Phytochemistry* 27:2801–2808.
29. Yan Y, Kohli A, Koffas MAG (2005) Biosynthesis of natural flavanones in *Saccharomyces cerevisiae*. *Appl Environ Microbiol* 71:5610–5613.
30. Jez JM, Bowman ME, Dixon RA, Noel JP (2000) Structure and mechanism of the evolutionarily unique plant enzyme chalcone isomerase. *Nat Struct Biol* 7:786–791.
31. Morita Y, et al. (2014) A chalcone isomerase-like protein enhances flavonoid production and flower pigmentation. *Plant J* 78:294–304.
32. Cheng AX, et al. (2018) Identification of chalcone isomerase in the basal land plants reveals an ancient evolution of enzymatic cyclization activity for synthesis of flavonoids. *New Phytol* 217:909–924.
33. Kaltenbach M, et al. (2017) Evolution of chalcone isomerase from a non-catalytic ancestor. *bioRxiv*, 10.1101/174128.
34. Gagne SJ, et al. (2012) Identification of olivetolic acid cyclase from *Cannabis sativa* reveals a unique catalytic route to plant polyketides. *Proc Natl Acad Sci USA* 109: 12811–12816.
35. Jiang W, et al. (2015) Role of a chalcone isomerase-like protein in flavonoid biosynthesis in *Arabidopsis thaliana*. *J Exp Bot* 66:7165–7179.
36. Abe I, Morita H (2010) Structure and function of the chalcone synthase superfamily of plant type III polyketide synthases. *Nat Prod Rep* 27:809–838.
37. Weng JK, Chapple C (2010) The origin and evolution of lignin biosynthesis. *New Phytol* 187:273–285.
38. Niesen FH, Berglund H, Vedadi M (2007) The use of differential scanning fluorimetry to detect ligand interactions that promote protein stability. *Nat Protoc* 2:2212–2221.
39. Shirley BW (1996) Flavonoid biosynthesis: 'New' functions for an 'old' pathway. *Trends Plant Sci* 1:377–382.
40. Zhang X, Abrahan C, Colquhoun TA, Liu CJ (2017) A proteolytic regulator controlling chalcone synthase stability and flavonoid biosynthesis in *Arabidopsis*. *Plant Cell* 29: 1157–1174.
41. Jørgensen K, et al. (2005) Metabolon formation and metabolic channeling in the biosynthesis of plant natural products. *Curr Opin Plant Biol* 8:280–291.
42. Jiang C, Kim SY, Suh DY (2008) Divergent evolution of the thiolase superfamily and chalcone synthase family. *Mol Phylogenet Evol* 49:691–701.
43. George JH, Hesse MD, Baldwin JE, Adlington RM (2010) Biomimetic synthesis of polycyclic polyprenylated acylphloroglucinol natural products isolated from *Hypericum papuanum*. *Org Lett* 12:3532–3535.
44. Yoo SD, Cho YH, Sheen J (2007) *Arabidopsis* mesophyll protoplasts: A versatile cell system for transient gene expression analysis. *Nat Protoc* 2:1565–1572.
45. Gietz RD, Woods RA (2002) Transformation of yeast by lithium acetate/single-stranded Carrier DNA/polyethylene glycol method. *Methods Enzymol* 350:87–96.
46. Pompon D, Louerat B, Bronine A, Urban P (1996) Yeast expression of animal and plant P450s in optimized redox environments. *Methods Enzymol* 272:51–64.
47. Jez JM, Noel JP (2002) Reaction mechanism of chalcone isomerase. pH dependence, diffusion control, and product binding differences. *J Biol Chem* 277:1361–1369.
48. Chen H, et al. (2008) Firefly luciferase complementation imaging assay for protein-protein interactions in plants. *Plant Physiol* 146:368–376.
49. Hellens RP, Edwards EA, Leyland NR, Bean S, Mullineaux PM (2000) pGreen: A versatile and flexible binary Ti vector for *Agrobacterium*-mediated plant transformation. *Plant Mol Biol* 42:819–832.
50. Clough SJ, Bent AF (1998) Floral dip: A simplified method for *Agrobacterium*-mediated transformation of *Arabidopsis thaliana*. *Plant J* 16:735–743.